Liquidlike atomic environments act as plasticity carriers in amorphous silicon

Michael J. Demkowicz[1,2,*] and Ali S. Argon[1]
[1]*Department of Mechanical Engineering, Massachusetts Institute of Technology, Cambridge, Massachusetts, 02139, USA*
[2]*MST-8: Structure-Property Relations, Los Alamos National Laboratory, Los Alamos, New Mexico, 87545, USA*
(Received 29 April 2005; revised manuscript received 29 September 2005; published 20 December 2005)

Molecular-dynamics simulation of amorphous silicon (a-Si) using the Stillinger-Weber potential reveals the existence of two distinct atomic environments: one solidlike and the other liquidlike. The mechanical behavior of a-Si when plastically deformed to large strain can be completely described by the mass fraction ϕ of liquidlike material in it. Specifically, samples with higher ϕ are more amenable to plastic flow, indicating that liquidlike atomic environments act as plasticity "carriers" in a-Si. When deformed under externally applied constant pressure, all a-Si samples converge to a unique value of ϕ characteristic of steady-state flow.

DOI: 10.1103/PhysRevB.72.245205 PACS number(s): 61.43.Dq, 61.43.Fs, 62.20.Fe, 81.05.Gc

I. INTRODUCTION

The motivation for this study originates in a desire to explain the unusually high resistance to plastic flow exhibited by a series of recently created nc-TiN/a-Si_3N_4 nanostructured ceramic composite coatings, some of which have shown indentation hardnesses in excess of that of nanocrystalline diamond thin films.[1] Detailed investigation has indicated that these coatings are made up of crystalline TiN grains 2–5 nm in diameter while the Si_3N_4 component is thought to exist in disordered intergranular layers of 1–3 atomic diameter thickness.[2] It has been suggested that at the appropriate proportions of these two components, the TiN grains are completely wetted by a monolayer of Si_3N_4.[3] Because of the small size of the TiN grains and the typically high lattice resistance of covalently bonded solids,[4] dislocation-mediated plasticity is not expected to play an important role in the mechanical behavior of nc-TiN/a-Si_3N_4 coatings. The plastic deformation behavior of the assemblage is therefore governed by the component whose ideal shear strength is lower.

The rise in plastic resistance associated with the increasing difficulty of nucleating and propagating dislocations as grain sizes decrease is a well-known effect in the study of polycrystalline metals[5,6] and has recently received considerable attention in large-scale atomistic simulation studies of metals.[7–10] Below grain sizes of about 10–20 nm, however, polycrystalline metals exhibit a reversal in the trend of increasing plastic resistance[10,11] as the rising proportion of intergranular regions makes large-scale plastic deformation by grain-boundary shear processes ever more favorable.[12] Therefore, the fact that—even at TiN grain sizes of 3.5 nm—nc-TiN/a-Si_3N_4 coatings do not show a reversal in the trend of rising plastic resistance with decreasing grain sizes[13] indicates that the intergranular regions in these materials are less amenable to plastic flow than the intergranular regions found in nanocrystalline metals. The reason for this difference likely arises because of the directional bonding environment of intergranular regions in nc-TiN/a-Si_3N_4.

The first step toward understanding plasticity in disordered intergranular layers is to develop insight into the plastic flow behavior of the intergranular material in its bulk amorphous or glassy form. The necessity of doing so has already been realized in the case of deformation of nanocrystalline metals, where deformation in intergranular layers is explicitly compared to deformation in metallic glasses.[14] Investigators of deformation in nanocrystalline metals benefit from a large body of knowledge that has been developed on plastic flow of metallic glasses.[15–21] A similarly large amount of research has been conducted on the mechanical properties of glassy polymers,[22–25] including their plastic response.[24,25] By comparison, however, the current state of knowledge on plasticity of covalent network materials is markedly deficient. This information is needed both in its own right as well as to explain the behavior of nanostructured ceramics.

Covalent network glasses, such as a-Si, a-Ge, SiO_2, B_2O_3, or alkali-modified glasses, should be studied separately from metallic glasses and glassy polymers because of fundamental differences in the type of atomic bonding environments envisioned in these three cases. Metallic glasses are usually modeled by collections of atoms interacting with spherically symmetric potentials that do not exhibit any directional nature.[19] Glassy polymers, on the other hand, exhibit strong directional bonds along polymer backbones, but the interactions of atoms not joined in this way (e.g., of atoms from different polymer chains) are once again modeled by relatively weaker spherically symmetric potentials.[22] Bonding between all atoms in covalent network glasses is of a strong and directional nature and so is qualitatively different from the two cases described above. The research presented here—already published in abbreviated form[26]—is a computer investigation of plastic deformation to strains much larger than the yield strain (i.e., to "large strain") in a system that incorporates the atomic bonding characteristics appropriate for directionally bonded network glasses.

II. THE MODEL SYSTEM

A faithful investigation of plasticity in the intergranular layers of nc-TiN/a-Si_3N_4 coatings would have to take into account a range of complex chemical interactions between all the elements that make up the material. Current *ab initio* methods are not yet capable of rapidly simulating atomic configurations of sufficient size ($\sim 10^3$–10^4 atoms) and on sufficiently long time scales ($\sim$1–10 ns) to address ques-

tions of fully developed low-temperature plasticity. On the other hand, well-tested empirical potentials for all the possible constituents of nanocrystalline ceramic coatings (e.g., for TiN) are largely unavailable. It is therefore convenient to conceive of a single-component model system capable of existing in disordered form as well as in a nanocrystalline form similar to that described for nc-TiN/a-Si_3N_4. The model system chosen should also have a well-tested empirical potential that explicitly incorporates the effects of directional bonding, as discussed in the Introduction. The above approximation requires that the chemically complex Si_3N_4 structural unit (which undergoes directional bonding to form a-Si_3N_4) be approximated by a unit without internal chemical structure and—in the case of a full nanocrystalline system—that the bonding differences between the structural units of the nondeforming crystallites and those of the intergranular material be ignored.

A clear choice for a model system that fulfills the above requirements is silicon. This material has a well-known amorphous form[27] and has been observed to form disordered intergranular layers[28] as well as nanocrystalline configurations that resemble those that are thought to describe nc-TiN/a-Si_3N_4.[29–31] Several empirical potentials to model it have been constructed and tested. The Stillinger-Weber (SW) potential for silicon[32] was chosen for this study from among the other most popular options[33–35] for four main reasons.

First, the SW potential is extremely well tested: its properties and behaviors have been studied by a number of independent investigators[36–40] whose work serves as a solid benchmark for further research. Second, SW Si has proved itself capable of producing amorphous configurations,[32,36] disordered intergranular layers for certain grain boundaries,[38] as well as fully nanocrystalline configurations that reproduce the essential structural features nc-TiN/a-Si_3N_4.[39] Third, the SW potential was chosen because it accounts for directional bonding in a particularly transparent manner. The potential V is a sum of interactions among pairs and triplets of atoms expressed as

$$V = \sum_{i<j} V_2(r_{ij}) + \sum_{i<j<k} V_3(r_{ij}, r_{ik}, r_{jk}), \tag{1}$$

where r_{ij} is the distance between atoms i and j. The two-body terms V_2 exhibit the intuitive characteristics of the Lennard-Jones potential, i.e., hard core repulsion at small distances followed by a potential minimum at some specified greater distance and subsequent convergence to zero at large distances. Unlike the Lennard-Jones potential, however, the two-body terms of the SW potential incorporate a weighting function that assures that the potential interaction along with all its derivatives become zero at some finite prespecified cutoff radius.

V_2 does not account for any directional bonding among atoms. That effect is entirely included in V_3, the potential of interaction of triplets of atoms. Its form is

$$V_3 = h(r_{ij}, r_{ik}, \theta_{jik}) + h(r_{ij}, r_{jk}, \theta_{ijk}) + h(r_{jk}, r_{ik}, \theta_{ikj}), \tag{2}$$

where θ_{jik} is the bond angle centered on atom i and bordered by the individual bonds $\mathbf{r}_{ij}$ and $\mathbf{r}_{ik}$. The bond angle-dependent term h is written

$$h(r_{ij}, r_{ik}, \theta_{jik}) = w(r_{ij}) w(r_{ik}) \left(\frac{1}{3} + \cos\, \theta_{jik} \right)^2, \tag{3}$$

where $w(r_{ij})$ denotes a weighting term—similar to the one encountered in the two-body terms V_2—that causes the three-body interaction along with all of its derivatives to vanish as r_{ij} approaches the cutoff radius. The last term is seen to be zero when the bond angle θ_{jik} has the value characteristic of bonds between nearest neighbors in the diamond cubic crystal, namely, about 109.5°. All other values of the bond angle result in the last term being positive. From this description it is clear that the SW potential can be thought of as essentially a Lennard-Jones potential that penalizes, through three-body interactions, bond angles deviating from those found in the diamond cubic crystal configuration. It is a natural extension of the well-known Keating potential[41] to situations where atoms need not simply oscillate about some specified equilibrium position but can also arbitrarily rearrange.

An immediate question that arises about the simple construction of the SW potential is whether it results in a completely accurate and precise description of the behavior of real silicon. The answer to this question cannot be unequivocal, for neither the SW potential nor any alternatives to it—being, after all, only *empirical* potentials—can do so perfectly. This shortcoming does not in any way invalidate their use, however, since many of them, including SW, do reproduce the behavior of silicon in broad brushstrokes. The SW potential, in particular, does better than most in reproducing the molten form of Si (an advantage that will be of importance in this study), coming closest to the experimentally observed nearest-neighbor coordination of about 6.4 (Ref. 42) with a predicted coordination of around 5 (Ref. 40). The environment-dependent interatomic potential[35] (EDIP) is further off the mark with a prediction of about 4.5.[43] The EDIP, however, predicts a coordination of 4.04 in amorphous Si (a-Si), which comes closer to the experimentally observed coordination of about 3.9 in a-Si produced by self-ion implantation[44] than that predicted by SW [4.14 (Ref. 36)]. Such variations are acceptable, however, and the results acquired from use of both SW and EDIP can be viewed as semiquantitative since both potentials avoid stark deviations from the properties of real silicon and neither predicts manifestly unphysical behaviors (it has been known for empirical potentials to give results that disagree *numerically* with experiments, but nevertheless reproduce the correct *trends* in behavior[45]). This lack of gross errors is the fourth reason for the choice of SW as a model material for this study.

III. METHODS

This study was conducted by molecular dynamics (MD) atomistic simulation[46] using a code made available by the Interfacial Materials Group at Argonne National Laboratory. This code implements system stress control using the Parinello-Rahman method,[47] which reduces to the method of Andersen in the special case of constant pressure.[48] During constant pressure deformation simulations, the system volume had to be rescaled occasionally to prevent pressure drift away from the intended value. A Gear predictor-corrector

integration scheme is used[46] with time increments of 3.87 fs, i.e., 0.05 times the characteristic time unit of the Stillinger-Weber potential of 76.6 fs. Temperature control is implemented using atomic velocity rescaling. This approach is acceptable because low-temperature plasticity is a phenomenon governed by the energetics of structure relaxations. The MD simulations applied in this study are therefore intended mainly as a means of relaxing the energy of atomic configurations, a procedure for which the details of how temperature is kept constant are of little importance.

This study has dealt with atomic configurations under periodic boundary conditions consisting of 4096 atoms, i.e., $8\times8\times8$ cubic unit cells of the diamond cubic configuration. The size of the system was chosen based on an analysis that assumed that, as in the case of metallic glasses[19] and amorphous polymers,[25] low-temperature plastic flow in a-Si occurs through a series of unit deformation events. The size of the a-Si system was made large enough to ensure that the character of unit plastic relaxation events would not be unduly affected by elastic interactions with its periodic images. This determination was accomplished on the basis of an argument used previously by Hutnik *et al.*[49] in the case of phenylene ring rotations in polycarbonate of bisphenol A. Using elementary continuum methods, it can be found that the excess elastic energy stored in a 4096-atom system due to the confinement of the unit event within the simulation cell is on the order of 0.7%. This result was obtained knowing that unit plastic events for SW a-Si occur within clusters consisting of about 10 atoms and that the Poisson ratio is in the range of 0.35–0.4 (Sec. IV). The assumptions used in this analysis were verified in an associated separate study of the atomic mechanisms of plasticity in a-Si.[50]

Plastic deformation simulations were carried out under volume-conserving plane strain[51] at constant volume as well as under constant zero pressure. Each initially equilibrated structure was deformed by applying a system-wide extension increment in the x direction ($d\varepsilon_x$) and the same amount of contraction increment in the y direction ($d\varepsilon_y$) while holding the z-direction length fixed (since the constant volume requirement in this loading mode requires $d\varepsilon_y=-d\varepsilon_x/(1+d\varepsilon_x)$, the amount of contraction increment applied in the y direction was actually very slightly less than extension in the x direction). After an atomic configuration is strained, it must be reequilibrated using MD relaxation. In the case of constant zero pressure-deformation simulations, the system volume must be allowed to change during the relaxation process, but is held fixed in the case of constant volume simulations. Equilibrium is considered to have been attained when macroscopic system characterizers, such as the pressure and internal energy, reach values that are steady to within the level of internal thermal fluctuations. When volume-conserving plane-strain increments with $d\varepsilon_x=10^{-3}$ are applied at $T=300$ K, this state is observed to have been attained after 1000 MD time increments. Extending the time of relaxation to 10 000 time increments did not result in any significant changes in the simulation results.

The stress tensor of the sample being deformed is of fundamental interest in the study of mechanical behavior. The full stress tensor for the simulated a-Si systems was calculated directly from the form of the assumed interatomic potential (Sec. II) as[52]

$$\tau_{ab}\mathcal{V}=\frac{\partial V}{\partial\varepsilon_{ab}}=\sum_{i=1}^{N}\sum_{j=i+1}^{N}\left(\frac{\partial V_2}{\partial r_{ij}}\frac{\partial r_{ij}}{\partial\varepsilon_{ab}}\right)+\sum_{i=1}^{N}\sum_{j=i+1}^{N}\sum_{k=j+1}^{N}\left(\frac{\partial V_3}{\partial r_{ij}}\frac{\partial r_{ij}}{\partial\varepsilon_{ab}}+\frac{\partial V_3}{\partial r_{ik}}\frac{\partial r_{ik}}{\partial\varepsilon_{ab}}+\frac{\partial V_3}{\partial r_{jk}}\frac{\partial r_{jk}}{\partial\varepsilon_{ab}}\right),\tag{4}$$

where $\partial r_{ij}/\partial\varepsilon_{ab}$ denotes the change of the distance between atoms i and j under variation in the applied strain increment component ε_{ab}, $\mathcal{V}$ is the total system volume, and N the total number of atoms in the simulation cell. The effect of nonzero temperature T on the stress state is accounted for by adding the term $mNk_BT\delta_{ab}$ to Eq. (4),[46] where m is the atomic mass, N the total number of atoms in the system, and k_B the Boltzmann constant. This term affects only the hydrostatic portion of the stress tensor.

To characterize the local stress level of an atomic environment, it is useful to decompose the system stress τ_{ab} in expression (4) into $i=1\ldots N$ components $(\tau_{ab})_i$ associated with atomic sites. Any such decomposition should satisfy the criterion

$$\tau_{ab}=\frac{1}{N}\sum_{i=1}^{N}(\tau_{ab})_i.\tag{5}$$

An atomic-level stress characterizer that does so is defined by

$$(\tau_{ab})_i\frac{\mathcal{V}}{N}=\frac{1}{2}\sum_{j=1}^{N}\left(\frac{\partial V_2}{\partial r_{ij}}\frac{\partial r_{ij}}{\partial\varepsilon_{ab}}\right)+\frac{1}{3}\sum_{j=1}^{N}\sum_{k=j+1}^{N}\left(\frac{\partial V_3}{\partial r_{ij}}\frac{\partial r_{ij}}{\partial\varepsilon_{ab}}+\frac{\partial V_3}{\partial r_{ik}}\frac{\partial r_{ik}}{\partial\varepsilon_{ab}}+\frac{\partial V_3}{\partial r_{jk}}\frac{\partial r_{jk}}{\partial\varepsilon_{ab}}\right).\tag{6}$$

The quantities $(\tau_{ab})_i$ are called the atomic-site stress tensors and serve as efficient characterizers of local internal stresses resulting from the disordered state of amorphous solids.[16,17,53] Note that while the summations in expression (4) are over all pairs and triplets of atoms occurring in the entire system, the summations in expression (6) are only over those pairs and triplets that contain atom i, which denotes the atomic site for which the local stress tensor $(\tau_{ab})_i$ is evaluated. The stresses at an atomic site, therefore, only involve contributions from direct energetic interactions with atomic sites within a radius dictated by the interaction cutoff distance of the SW potential[32] and can therefore be interpreted as measures of local structure distortion.

Because a-Si is an isotropic material, the results of mechanical deformation simulations are conveniently stated in terms of the pressure p and deviatoric $\bar{\sigma}$ components of the stress tensor $\boldsymbol{\tau}$.[51] These components are defined as

$$p(\boldsymbol{\tau})=-\tfrac{1}{3}tr(\boldsymbol{\tau})\tag{7a}$$

$$\bar{\sigma}(\boldsymbol{\tau})=\left|\boldsymbol{\tau}-\tfrac{1}{3}tr(\boldsymbol{\tau})\mathbf{I}\right|,\tag{7b}$$

where tr stands for the tensor trace and $\mathbf{I}$ for the identity tensor. Deviatoric stress accounts for all shearing stresses and excludes all dilatational stress components. Both pressure and deviatoric stress can be computed for the system-wide stress tensor as well as for all atomic site stress tensors.

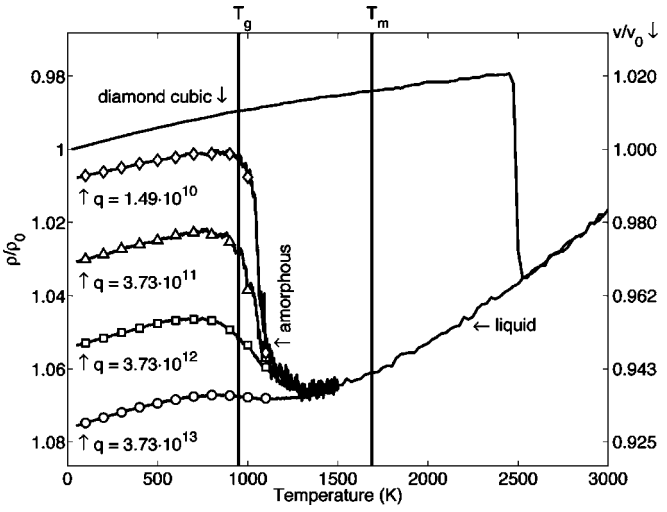

FIG. 1. The simulated c-Si system must be overheated by over 800 K above its accepted melting temperature before liquefying. Upon melting, it undergoes volume contraction. When quenched, molten Si vitrifies at a glass-transition temperature of about 950 K. The final density of the resulting a-Si depends sensitively on the applied rate of quenching q. All quench rates are in Kelvin per second. Densities and volumes are shown scaled by the density and specific volume of SW c-Si at zero temperature and pressure: $\rho_0 = 2323.8\ \mathrm{kg/m^3}$ and $v_0 = 4.3033 \times 10^{-4}\ \mathrm{m^3/kg}$.

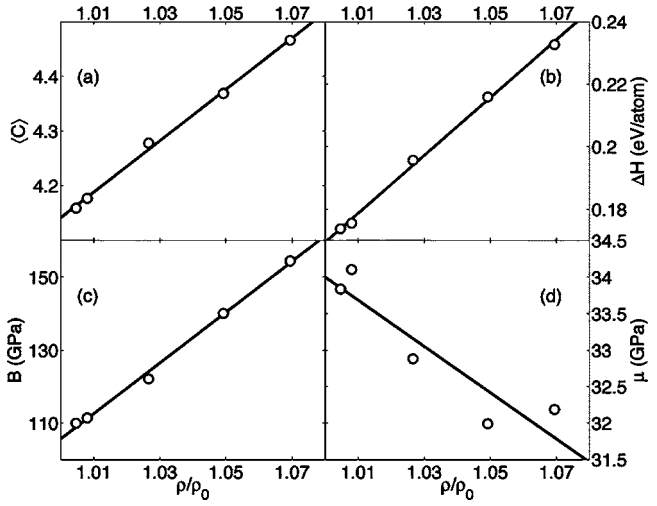

FIG. 2. The relative densities ρ/ρ_0: (a) average coordinations $\langle C \rangle$, (b) excess enthalpies ΔH, as well as (c) bulk and (d) shear moduli B and μ of a-Si approach asymptotic values for ever slower quenching. The rate of approach to the asymptote is the same for all these quantities, as evidenced by their approximately linear dependence on each other.

Although system-wide p and τ_{ab} are averages over the volume of corresponding atomic-site quantities, the system-wide deviatoric stress, however, is not the average over the volume of atomic-site deviatoric stresses. Rather, it is the deviatoric component of the volume average atomic site stress tensors. Deviatoric strain $\bar{\varepsilon}$ is computed from the strain tensor $\boldsymbol{\varepsilon}$ analogously to deviatoric stress.

IV. MELTING AND QUENCHING BEHAVIOR

The a-Si configurations studied here were created by melting initially diamond cubic crystalline Si (c-Si) structures and then quenching them at a number of different rates using constant zero-pressure MD simulations. The melting and quenching behavior of SW Si is summarized in Fig. 1. As expected, due to the absence of sites enabling easy nucleation of the liquid phase,[54] the crystalline structure had to be overheated to ~2500 K before it melted, i.e., past the accepted melting temperature for SW Si of ~1690 K (Ref. 55) (the evaluation of the thermodynamic melting temperature by MD simulation requires allowing for free temperature adjustments until a state of equilibrium is attained in a mixture of coexisting solid and liquid phases of the material). Upon melting, the system contracted by ~5.4%, in agreement with the intended design of the SW potential.[32] This contraction upon melting is a well-verified characteristic of Si.[56] It is typical of materials that have open crystalline structures.[57]

When quenched, liquid silicon undergoes a transition to a disordered solid form at ~950 K. The densities of the final a-Si structures obtained by quenching are highly sensitive to the quench rate used in creating them. The lowest density a-Si structures approach a density slightly higher than that of c-Si as shown in Fig. 1 and are obtained using the slowest quench rates. Faster quench rates yield higher density structures. This quench-rate dependence of a-Si densities is paralleled by the quench rate dependence of average atomic coordinations of a-Si. Fast quenching gives rise to higher atomic coordination values, whereas slow quenching results in lower coordinations, approaching a coordination slightly higher than that of c-Si. Both the densities and coordination numbers approach asymptotic values when extrapolated to infinitely slow quenching. Furthermore, the rate of approach to the asymptote is the same in both cases, as confirmed by their linear dependence on each other, shown in Fig. 2(a). Similar quench rate dependencies are observed for the excess enthalpies and isotropic elastic constants (bulk and shear moduli) of a-Si. As demonstrated in Figs. 2(b)–2(d), all of these quantities are therefore conveniently parametrized in terms of the densities of the quenched a-Si structures.

Characterization of the atomic structures of the variously quenched a-Si configurations is accomplished by using radial and angular distribution functions (RDFs and ADFs). Figure 3 plots these functions for "as-quenched" a-Si structures of four different densities, i.e., produced using four different rates of quenching. The RDFs [shown in Fig. 3(a)] all exhibit distinct nearest-neighbor peaks and a split-second nearest-neighbor peak. The nearest-neighbor distance for low-density systems is sharper and higher than in the case of high-density ones. Furthermore, the lower-length section of the split-second nearest-neighbor peak is attenuated for low-density systems while the higher-length section is intensified. The opposite is true for high-density systems. The ADFs [given in Fig. 3(b)] show an intensification of the peak at ~109.5° (the characteristic bond angle of the diamond cubic crystal configuration) with decreasing density. These changes in structure are consistent with a tendency of a-Si to gradually become more like c-Si when allowed to relax for increasing periods of time, while still retaining its amorphous structure.

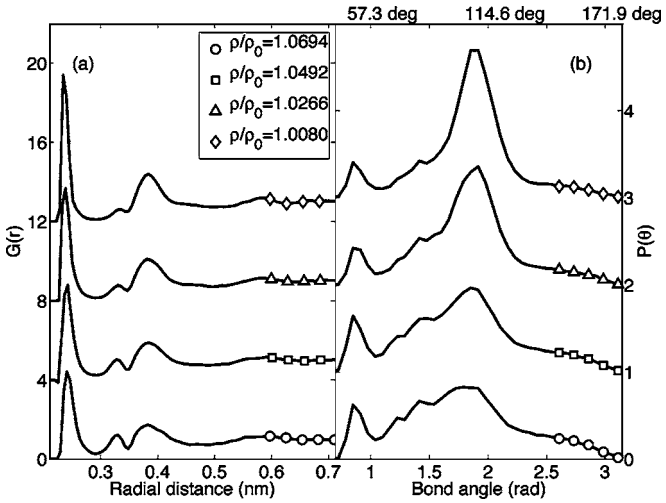

FIG. 3. The average atomic-level structures associated with differently quenched a-Si systems can be characterized by (a) radial distribution functions (RDFs) and (b) nearest-neighbor angular distribution functions (ADFs). The plots shown above have been displaced in the y-axis for clarity.

Further insight into the nature of atomic environments in a-Si structures of different densities can be obtained by investigation of the atomic level stresses introduced in Sec. III. Figures 4(a) and 4(b) show histograms of atomic-level pressures and deviatoric stress components for a typical a-Si system. These quantities exhibit a large spread of values, indicating that, much as in the case of metallic glasses,[17] individual atomic environments in a-Si are far more distorted than the level of overall system stress (i.e., the average of atomic stresses, Sec. III) would indicate. Using dimensional

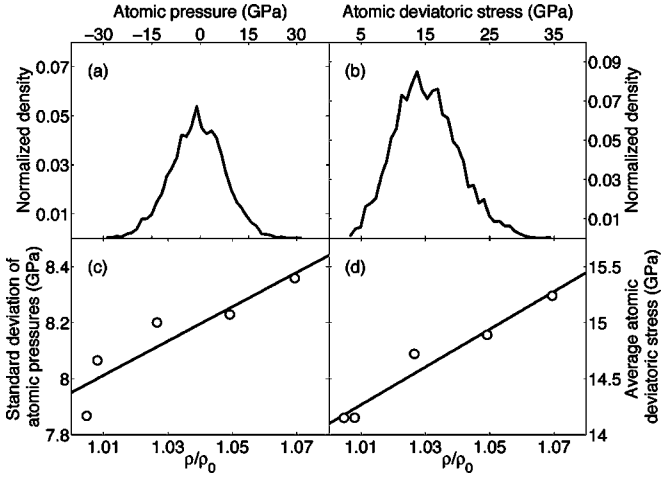

FIG. 4. Typical distributions of atomic-level (a) pressures $p(\boldsymbol{\tau}_i)$ and (b) deviatoric stresses $\bar{\sigma}(\boldsymbol{\tau}_i)$ demonstrate that local atomic environments exhibit a broad range of stress states, even though the average system stress may be close to zero. The largest atomic-level stresses approach the approximate decohesion-level stress for SW Si of about 37.8 GPa. The (c) standard deviation of atomic-level pressures and (d) average atomic deviatoric stress levels in a-Si structures are directly correlated to the quench rates used to create them, as evidenced by the linear dependence of these quantities on density.

analysis, the characteristic length and energy scales of the Stillinger-Weber potential[32] can be used to calculate the characteristic stress scale[46] of ~37.76 GPa, which is approximately the same as the decohesion stress of SW Si. Figures 4(a) and 4(b) demonstrate that the stress level of certain atomic environments approaches that of decohesion. Figures 4(c) and 4(d) show that the standard deviation of atomic pressures and the average of atomic deviatoric stresses demonstrate a distinct dependence of the average level of distortion in atomic environments on quench rate (recall that the average of atomic pressures simply gives the overall system pressure as explained in Sec. III). The higher atomic-site stresses in quickly quenched structures can be viewed as the principal cause for the larger excess enthalpies of such structures [Fig. 2(b)], the latter being related to the elastic strain energies associated with the atomic-site stresses.

To compare the results of the melting and quenching simulations presented here with experimental findings, it is necessary to observe that the quench rates used in MD simulations are several orders of magnitude higher than the highest ones typically attainable in practice. Therefore, the a-Si samples studied in experiments should be thought of as extremely well relaxed and only the best-relaxed a-Si systems prepared by MD should be compared to them. Table I lists several parameters evaluated for the slowest-quenched system created as part of this study. It demonstrates acceptable agreement with experimental results as well as with previous simulations. It should be noted that the best relaxed system obtained in this study reached a lower value of potential energy than all previous simulations known to the authors, including ones that resorted to highly intricate or unphysical methods.[58]

At first glance, the melting and quenching behavior of Si stands in stark contrast to that of metals, which expand upon melting and yield glasses of increasing density at slower quench rates.[60] Nevertheless, it is clear that both a-Si and metallic glasses exhibit a fundamental similarity in their quench rate dependence: in both cases slower quenching leads to the creation of disordered solids whose character, as determined by densities, coordinations, etc., approaches that of the parent crystalline phase while fast quenching produces structures similar to the liquid phase.

V. LOCAL STRUCTURE OF ATOMIC ENVIRONMENTS

The mutual interrelationship of a-Si densities, coordinations, and excess enthalpies as well as structural features as described by RDFs, ADFs, and atomic-level stress distributions strongly suggests that variations in these quantities can be explained using a single, well-defined atomic-level structure descriptor. To find this descriptor, a characterization of the local structure of atomic environments in a-Si was proposed based on the nearest-neighbor bond angles at each atomic site.[26] Every atom i in the a-Si systems studied here forms bonds with its m_i nearest-neighbor atoms. These bonds define $n_i=\frac{1}{2}m_i(m_i-1)$ nearest-neighbor bond angles for atom i. Call these bond angles θ_{ij}, $j=1\ldots n_i$ and define their mean and standard deviation as

TABLE I. The characteristics of the best-quenched a-Si samples described in this study[26] are in good agreement with experiment and previous simulations.

	Best-quenched a-Si	Previous simulations	Experiment
Coordination	4.15	4.14[a]	3.8–4.1[d]
Bulk modulus	110 GPa	106 GPa[b]	~100 GPa[e]
Shear modulus	34 GPa	33 GPa[b]	~38 GPa[e]
Potential energy	–4.16 eV/atom	–4.12 eV/atom[c]	N/A

[a]Reference 36.
[b]Reference 37.
[c]Reference 58.
[d]Reference 44.
[e]Reference 59.

$$\mu_i = \frac{1}{n_i}\sum_{j=1}^{n_i} \theta_{ij} \tag{8a}$$

$$\sigma_i^2 = \left(\frac{1}{n_i}\sum_{j=1}^{n_i} \theta_{ij}^2\right) - \mu_i^2. \tag{8b}$$

The quantities μ_i and σ_i can be computed for the atomic environment of each individual atom i. They can therefore act as effective characterizers of the local structure of atomic bonding environments.

The distributions of the values of μ_i and σ_i for all 4096 atoms in a-Si systems of differing densities are shown in Figs. 5(a) and 5(b). It is immediately apparent that these distributions are bimodal. Moreover, the distributions for a-Si systems of differing densities exhibit different peak heights, but no change in peak positions or abatement of bimodality. Plotting μ_i and σ_i against each other for all 4096 atoms in a typical a-Si system shows in Fig. 6 that the two quantities are correlated. In particular, the distribution peaks in Fig. 5 are made up of contributions from the same atomic environments. The characterization of local structure of atomic environments based on the values of μ_i and σ_i, therefore, allows for their separation into two distinct types, which, for reasons explained below, were named "solidlike" and "liquidlike," following the terminology introduced by Cohen and Grest.[61]

Once all atomic environments in an a-Si system have been classified by the above analysis, they could be viewed, for all practical purposes, as two separate species, each with well-defined physical properties. In particular, RDFs and ADFs can be found for each one. This determination was accomplished in this study by separately accumulating the contributions of solidlike and liquidlike atomic environments to the overall system RDF and ADF. To approximate the RDFs and ADFs for "pure" solidlike a-Si and liquidlike a-Si, contributions were considered only from those atomic environments whose nearest-neighbor atoms had atomic environments of the same type. The results are presented in Fig. 7 and immediately indicate why the two types of atomic envi-

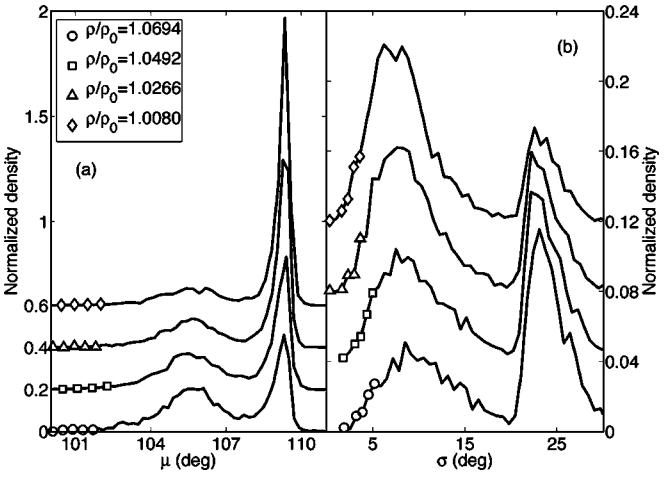

FIG. 5. The distributions of (a) means μ [Eq. (8a)] and (b) standard deviations σ [Eq. (8b)] of nearest-neighbor bond angles for the atomic environments in a-Si systems of differing densities are bimodal. Systems of differing densities exhibit different relative peak heights, but no shift in the peak positions or abatement of bimodality. The plots shown above have been displaced in the y-axis for clarity.

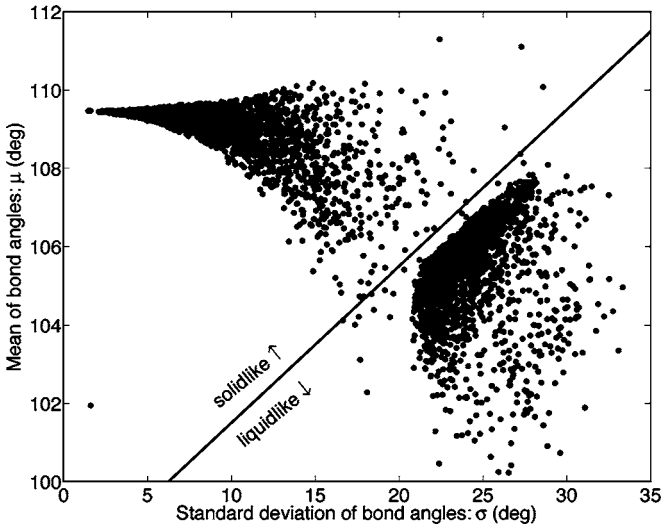

FIG. 6. Atomic environments in a-Si are naturally separated into two distinct types based on clustering in the means μ [Eq. (8a)] and standard deviations σ [Eq. (8b)] of the nearest-neighbor bond angles that surround them.

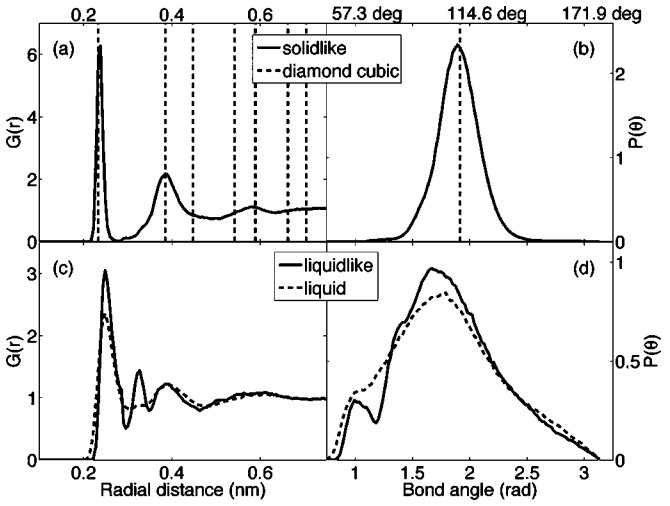

FIG. 7. Comparison of the RDFs and ADFs of the two distinct atomic environments of a-Si with the RDFs and ADFs of diamond cubic c-Si and molten Si allow these environments to be identified as "solidlike" (a, b) and "liquidlike" (c, d).

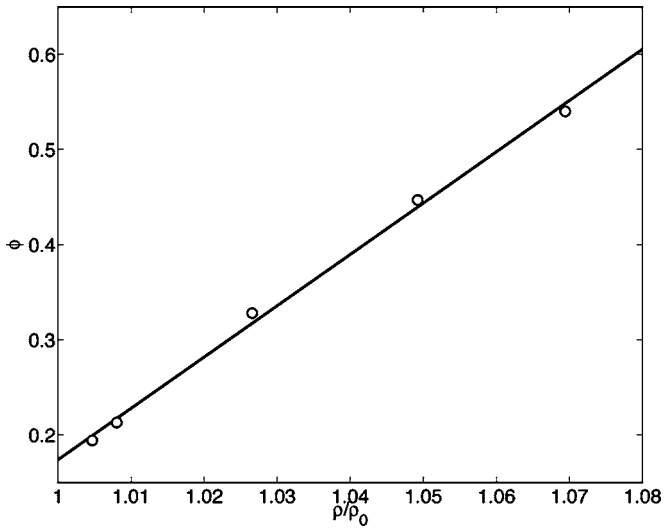

FIG. 8. The mass fraction ϕ of liquidlike atomic environments present in variously quenched a-Si systems depends linearly on their relative density ρ/ρ_0. The reference density is that of SW c-Si at zero temperature and pressure: $\rho_0=2323.8$ kg/m^3.

ronment were termed solidlike and liquidlike: inspection of their RDFs and ADFs indicates that one has a structure that resembles that of molten Si while the other more closely resembles diamond cubic silicon (especially in the ADF). The liquidlike and solidlike character of the two distinct atomic environments found in a-Si is further reinforced by their average densities, coordinations, as well as two- and three-body contributions (see Sec. II) to atomic binding energies, presented in Table II. Each of these quantities is in close agreement for diamond cubic c-Si and solidlike a-Si as well as for liquid Si and liquidlike a-Si.

When the number of liquidlike and solidlike atomic environments in a given a-Si system is known, a unique mass fraction of each environment in that system can then be defined; it is simply the ratio of the number of atoms with that environment to the total number of atoms in the system. Furthermore, since there are only two unambiguously distinguishable atomic environments in a-Si, the sum of their mass fractions must equal unity. Consequently, the "composition" of each a-Si system can be summarized by the mass fraction of just one of the environments. It will be convenient, for reasons explained later, to choose the mass fraction of liquidlike atomic environments ϕ as such a descriptor. Figure 8 shows that there is an approximately linear dependence of ϕ in as-quenched a-Si systems on their densities. Given that such properties as coordination, excess enthalpy, and isotropic elastic constants exhibit an approximately linear dependence on system density (see Sec. IV), it is clear that they also exhibit a corresponding linear dependence on ϕ. The composite properties of a-Si systems with a given ϕ thus arise from the rule of mixtures applied to the properties of liquidlike and solidlike atomic environments alone. More precise determinations of composite properties are the aim of homogenization theory.[62]

The distribution of each environment throughout the simulation cell was studied using standard two-point correlation functions,[62] the coarseness characterizer of Lu and Torquato,[63] autocorrelations like those used in the study of surface morphology,[64] and various cluster shape measures.[65] In the course of these studies, no evidence was ever found for nonhomogeneity or anisotropy in the distribution of these two atomic environments. A coherence length for each environment spanning approximately two interatomic distances was the only form of nonuniformity that was observed. In particular, neither of the two types of atomic environments exhibited any tendency to cluster into phase domains. These conclusions are confirmed by direct visualizations of the distribution of liquidlike and solidlike atomic environments in a-Si configurations. Figure 9 shows two such visualizations for systems of differing ϕ.

It must be stressed that both the solidlike and liquidlike atomic environments are forms of solid amorphous Si. The

TABLE II. Comparison of diamond cubic Si and liquid Si with solidlike a-Si and liquidlike a-Si (Ref. 26) via average coordination, density, and two and three-body contributions to atomic binding energies (E_b).

	Diamond cubic Si ($T=0$ K)	Liquid Si ($T=1690$ K$\approx T_m$)	Solidlike a-Si ($T=300$ K)	Liquidlike a-Si ($T=300$ K)
Coordination	4	5.13±0.86	4.00±0.06	4.97±0.40
Density (kg/m^3)	2324	2386	2256	2554
E_b two-body (eV)	−8.67	−9.93±0.95	−8.82±0.37	−10.45±0.52
E_b three-body (eV)	0	3.60±1.21	0.91±0.54	4.16±0.89

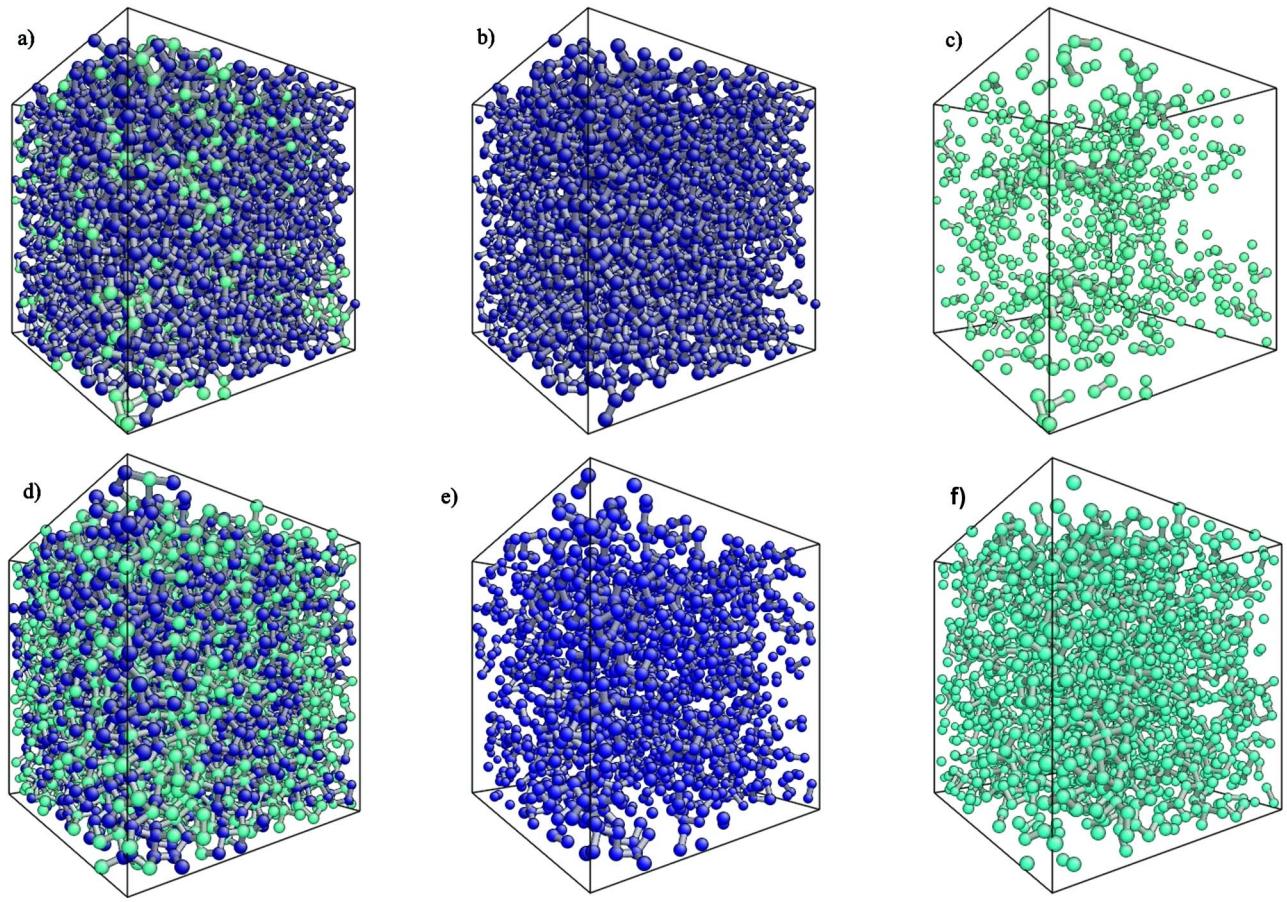

FIG. 9. (Color online) Visualizations of the composition of two a-Si systems in terms of solidlike (dark) and liquidlike (light) atomic environments are shown above. (a–c), show, respectively, all atomic environments, only the solidlike ones, and only the liquidlike ones for a system with specific density $\rho/\rho_0=1.008$. (d–f) are the corresponding depictions for a system with $\rho/\rho_0=1.069$. As expected, the denser system has a higher liquidlike mass fraction ϕ. These visualizations demonstrate that the distribution of solidlike and liquidlike atomic environments in as-quenched a-Si systems is uniform and isotropic.

solidlike form lacks long-range order despite a short-range resemblance to the diamond cubic structure. The liquidlike form bears a structural similarity to molten silicon, but it is, nonetheless, vitrified. Furthermore, precedents for glassy materials whose structures resemble either the solidlike or liquidlike atomic environments in a-Si already exist in the literature.[66] Specifically, the solidlike atomic environment is well described as a continuous random network (CRN).[67] This model was originally proposed for oxide glasses and claims that the nearest-neighbor environment of each atom is topologically the same as it would be in its crystalline configuration. An immediate consequence of this description is that the average coordination of atoms in a CRN must be the same as that of the crystal, as is indeed the case for solidlike a-Si (Table II). Long-range order is lost in the CRN model primarily because of variations in nearest-neighbor bond angles, but not in nearest-neighbor bond lengths, which are thought to be too stiff to undergo significant changes. The RDF and ADF for the solidlike atomic environment (Fig. 7) agree with these assumptions.

The liquidlike atomic environment of a-Si, on the other hand, bears certain characteristic features of dense random packing (DRP).[68] Specifically, its short-range atomic ordering differs topologically from that of c-Si, as evidenced by its on-average higher and broadly distributed coordination number (Table II). The broadened nearest-neighbor peak in the RDF and wide distribution of nearest-neighbor bond angles in the ADF (Fig. 7) for liquidlike a-Si reinforce this conclusion. The DRP model, moreover, bears a close resemblance to the arrangement of atoms in a metallic or hard-sphere liquid,[69] with the notable exception that the DRP exhibits a split peak in the second nearest-neighbor shell, whereas simple liquids have just one smooth second nearest-neighbor peak.[46] These characteristics are perfectly mirrored in the relation of liquidlike a-Si to liquid Si (Fig. 7). Of course, the liquidlike a-Si environment is not strictly a dense random packing: the DRP model was originally developed to describe ball-bearing packings and metallic glasses, both of which generally have close-packed crystalline structures (coordination of 12) and disordered states with average coordinations around 11. It is amazing, therefore, that the other characteristics of DRP described above hold so well for liquidlike a-Si, whose average coordination is close to 5 (Table II). This agreement suggests that the crucial link between DRP and liquidlike a-Si is their relation to the structure of the corresponding molten state of the material each aims to represent.

VI. DEFORMATION TO LARGE STRAIN BY MD AT CONSTANT VOLUME

The mechanical behavior of a-Si was probed by deforming four selected systems from their initial as-quenched state to large strain. Each of these systems had a different density, correlated to the rate of quenching used to create it. Deformation was carried out as described in Sec. III using MD simulation at a temperature of 300 K, well below the glass-transition temperature of 950 K, i.e., in the regime of low-temperature plasticity.[70] The stress-strain and pressure-strain curves obtained from these deformation simulations are shown in Figs. 10(a) and 10(b). They exhibited considerable jerkiness due to the discrete nature of the atomic structure rearrangements responsible for plasticity and the small size of the simulation cell. Averaging of stress-strain curves from many deformation simulations of systems with similar densities and quenching histories smoothes out this jerky response while reinforcing general deformation characteristics, such as the level of yield and steady-state flow stress. The smoothness of stress-strain curves obtained experimentally through the study of macroscopic systems is a consequence of such ensemble averaging of discrete atomic-level events.

Deformation of as-quenched structures of differing densities shows that the character of plastic behavior is crucially dependent on system density. For the system of lowest density, three significant features of deformation behavior are immediately discernable. First, elastic loading (albeit nonlinear) terminates with a sharp yield phenomenon. Second, initial yield is followed by significant strain softening [Fig. 10(a)]. Third, plastic deformation is accompanied by a dramatic drop of system pressure well below zero [Fig. 10(b)]. The first two of these three phenomena have also been observed in simulations[20,21] and experiments[71] on aged metallic glasses, but the third is entirely different. The pressure drop during deformation at constant volume corresponds to volume contraction in constant pressure deformation and stands in stark contrast to the behavior of metallic glasses, which expand during deformation. Figure 10(a) also shows that no well-defined yield point is observed for high-enough initial densities. Furthermore, high-density systems do not exhibit the pressure drop apparent in the deformation behavior of low-density systems. Instead, their pressure increases drastically, corresponding to a system dilatation under constant pressure. Unlike in metallic glasses where the pressure and deviatoric stress attain steady state at the same strain, the pressure in these dense structures stabilizes at higher strain than does the deviatoric stress.

The behavior described above suggests that a-Si systems undergo some structural evolution as they deform. First, the strain softening and pressure drop of systems with low initial density indicates a gradual transition to a denser, easily flowing state. Lack of sharp yielding for initially dense systems reinforces the view that denser structures flow more easily. Meanwhile, the prolonged change in pressure during deformation of these systems indicates that in the flow state, kinetic equilibrium is established between structural components of varying density. All of these changes are well described by the separation of a-Si into solidlike and liquidlike atomic environments (Sec. V). Figure 10(c) shows the

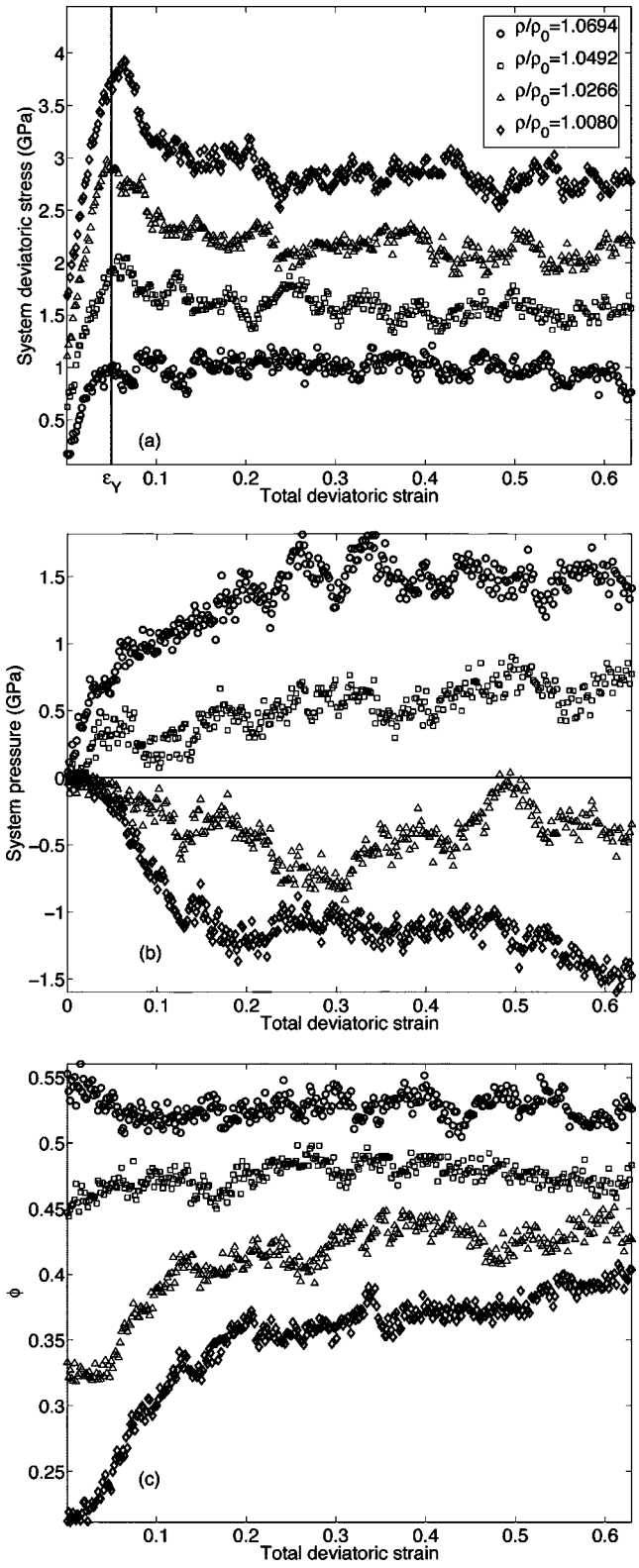

FIG. 10. The plots above show the variations of (a) deviatoric stress $\bar{\sigma}(\boldsymbol{\tau})$, (b) pressure $p(\boldsymbol{\tau})$, and (c) mass fraction of liquidlike atomic environments ϕ as functions of the deviatoric component $\bar{\varepsilon}(\boldsymbol{\varepsilon})$ of the total externally applied strain for four a-Si structures of differing densities undergoing large-strain plastic flow under constant volume. The data series in (a) all begin at the origin, but have been offset in increments of 0.5 GPa for clarity.

change in ϕ during deformation of the four a-Si systems of different densities. Each structure starts out with a different liquidlike fraction that changes during deformation and levels off when steady-state flow is reached. The smallest initial fraction of liquidlike atomic environments is found in the best-annealed structures and increases in the course of strain softening, in agreement with the observed drop in pressure in those structures (the liquidlike environment is denser than the solidlike one; Sec. V). Increasing volume fractions of liquidlike atomic environments can therefore be associated with decreasing resistance to plastic flow of a-Si structures. Conversely, structures with low liquidlike fractions can be expected to exhibit a high initial resistance to plastic flow.

VII. MASS FRACTION ϕ OF LIQUIDLIKE ATOMIC ENVIRONMENTS AS PLASTICITY CARRIER IN a-Si

Based on the above observations, mass fractions ϕ of liquidlike components can be viewed as "plasticity carriers" for a-Si in analogy with dislocation densities in c-Si.[72] For this comparison to hold, however, it is necessary that annealing "ages" the structure, making it more resistant to initiation of plastic flow while plastic deformation "rejuvenates" it, making it more amenable to plastic flow. To probe this issue, an initially well-relaxed a-Si structure was plastically deformed to high strain, allowing it to develop a significant liquidlike mass fraction ϕ as shown in Fig. 11. This a-Si system was then plastically deformed back to its initial configuration by straining it in the reverse direction to that of initial loading. Figure 12 demonstrates that because the system contained a high liquidlike mass fraction at the beginning of reverse deformation, it did not exhibit a yield phenomenon, confirming that its internal atomic arrangement had indeed been rejuvenated.

Upon returning to its original shape, the a-Si system was annealed for nearly 4 ns at a temperature of 925 K (i.e., just below the glass transition temperature) and slowly quenched. As illustrated in Fig. 13, most of the liquidlike mass fraction accumulated as a result of previous plastic deformation was thereby removed. Next, the system was once again plastically deformed to high strain. Figure 14 shows that the system then exhibited a distinct yield phenomenon along with strain softening and an increase in the liquidlike volume fraction. It may therefore be concluded that annealing does indeed age the a-Si structure, resulting in an increased resistance to plastic flow. The identification of the mass fraction of liquidlike atomic environments ϕ as the plasticity carrier for a-Si is therefore a valid mesoscopic description of the internal structure changes in a-Si during plastic deformation. It is a good candidate for an internal variable characterizing the state of the material in a possible continuum description of plasticity in a-Si.[73,74]

VIII. DEFORMATION TO LARGE STRAIN BY MD AT CONSTANT ZERO PRESSURE

In the constant volume simulations of plastic flow presented above, ϕ fails to converge to a unique value during steady-state flow for the four density structures considered in this study [Fig. 10(c)]. This apparent discrepancy is removed when the possibility of direct dependence of mechanical properties on pressure is taken explicitly into account. In constant volume simulations, the system pressures are allowed to change. They converge to different steady-state values in the case of each of the four density structures considered [Fig. 10(b)]. Plastic deformation in these structures was therefore simulated once again, this time by MD at constant zero externally applied pressure (Sec. III), though also at a temperature of 300 K. The same strain increments were ap-

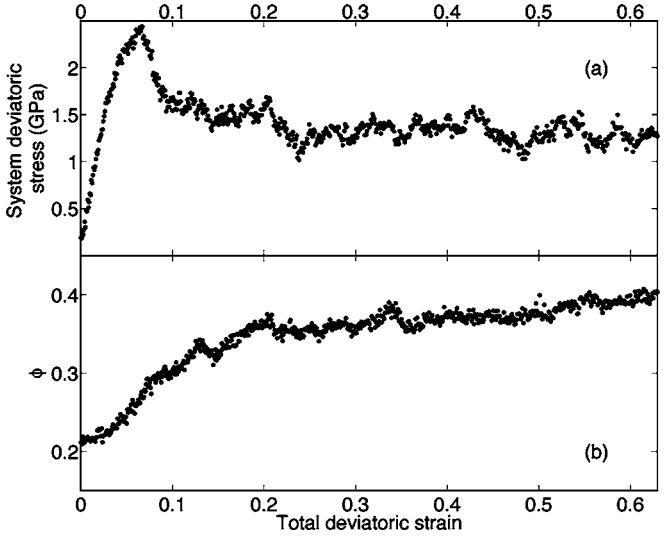

FIG. 11. An initially well-annealed a-Si system has a low liquidlike mass fraction. It exhibits a distinct yield phenomenon, and strain softens as the liquidlike mass fraction increases.

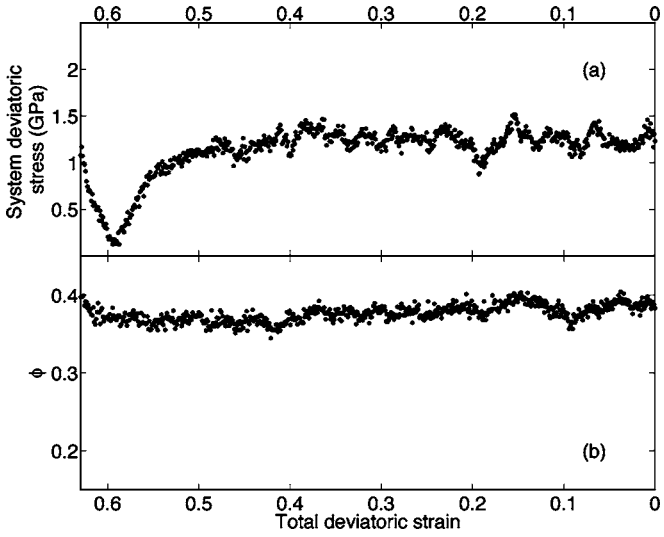

FIG. 12. The deformed a-Si system from Fig. 11 has an initially high liquidlike mass fraction, created as a result of plastic deformation. Upon unloading, it did not exhibit a yield phenomenon or strain softening. The values of deviatoric stress in the dip observed upon deforming in the reverse direction are attributed to elastic unloading and reloading combined with a Bauschinger effect. Note that the deviatoric stress $\bar{\sigma}(\tau)$ is an intrinsically positive quantity (Sec. III).

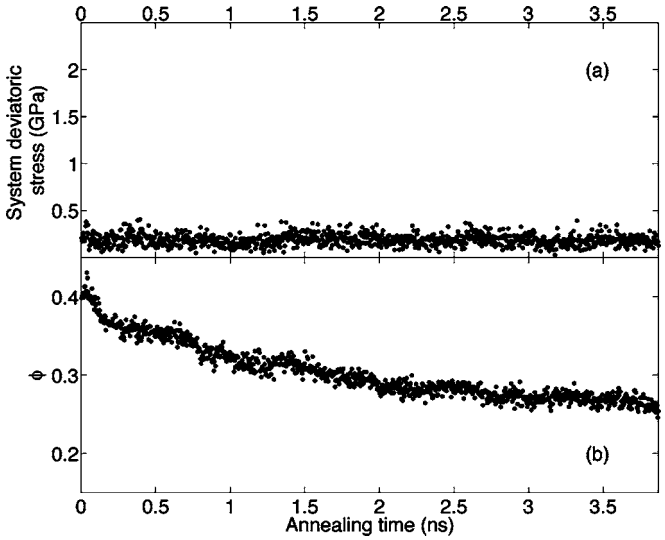

FIG. 13. After the a-Si structure in Figs. 11 and 12 had been cyclically deformed, it was annealed at 925 K for nearly 4 ns, removing much of the liquidlike mass fraction that had previously accumulated as a result of plastic deformation.

plied to the a-Si structures as before, except that the total system volume was allowed to change during the subsequent relaxation so as to maintain approximately zero constant externally applied pressure. (The MD algorithm used does not yield a strictly constant pressure, but rather one that oscillates about the prescribed value. The standard deviation of pressure oscillations in the deformation simulations presented here was just under 60 MPa.). The results are presented in Fig. 15. Comparison of Figs. 15(a) and 10(a) shows that there is no appreciable difference in the behavior of the deviatoric stress from that in the case of constant volume deformation. As expected, the density changes under constant pressure [Fig. 15(b)] mirror the pressure changes under constant volume [Fig. 10(b)] and the values of ϕ undergo similar evolution in both cases [Figs. 10(c) and 15(c)]. Unlike in the constant volume simulations, however, both the system volumes and liquidlike mass fractions in the constant pressure simulations eventually converge to unique steady-state flow values. These results confirm that the differing liquidlike mass fractions ϕ at steady-state flow are indeed due to their direct pressure dependence.

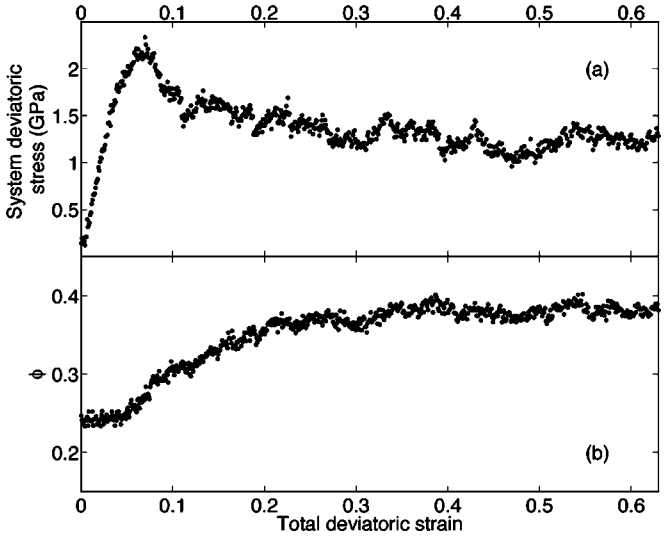

FIG. 14. Once the liquidlike mass fraction of the a-Si system cyclically deformed in Figs. 11 and 12 was reduced by annealing (Fig. 13), the system once again exhibited a distinct yield phenomenon and strain softening accompanied by an increasing liquidlike mass fraction upon plastic deformation.

IX. LOCALIZATION OF ATOMIC ENVIRONMENT TRANSFORMATIONS

Figures 10(c) and 15(c) demonstrate that the attainment of steady-state flow requires that structure transformations take place between the solidlike and liquidlike atomic environments. Some insight into the character of these transformations can be gained by visualizing the regions within deformed a-Si systems that have undergone transformations in the type of their atomic environments (from solidlike to liquidlike or vice versa) during the course of plastic flow. Figure 16(a) shows that during plastic deformation of an a-Si system with an initially high value of ϕ there appears not to be any tendency for atomic environment structure transformations to localize exclusively within any particular region of the simulation cell. In that system, therefore, the distribution of liquidlike and solidlike environments remains uniform. In the case of an a-Si system with an initially low ϕ, however, these transformations occur predominantly within a relatively distinct plane spanning the simulation cell and oriented along a direction of maximum resolved shear stress, as Fig. 16(b) demonstrates. The rising proportion of liquidlike mass fraction, therefore, is not uniformly distributed throughout this system. There should, however, exist a length scale sufficiently short such that the distribution of liquidlike environments across it can be considered approximately uniform on average. A unique average local flow stress as a function of ϕ would then exist for chunks of a-Si material of such characteristic length.

The above observations suggest two hypotheses. First, solidlike atomic environments are transformed into liquidlike ones (and vice versa) by spatially localized structure changes. Transformation of atomic environments by delocalized structure changes would not allow for the clustering of transformed material into a distinct zone, as in Fig. 16(b). Second, liquidlike atomic environments decrease the local resistance of a-Si to plastic flow. Structure transformations occur preferentially within the distinct zone of Fig. 16(b) because a higher ϕ has been created there as a result of previous transformations while the material outside that zone is locally more resistant to plastic flow. On the other hand, there are enough liquidlike environments initially distributed throughout the system in Fig. 16(a) to enable structure transformations to initiate practically anywhere. These two hypothesis are essentially concerned with the existence and character of discrete mechanisms of plastic flow in a-Si and the local conditions of its onset.

X. DISCUSSION AND CONNECTION WITH EXPERIMENTAL FINDINGS

It was shown in Secs. IV and V that liquidlike and solidlike atomic environments have well-defined physical proper-

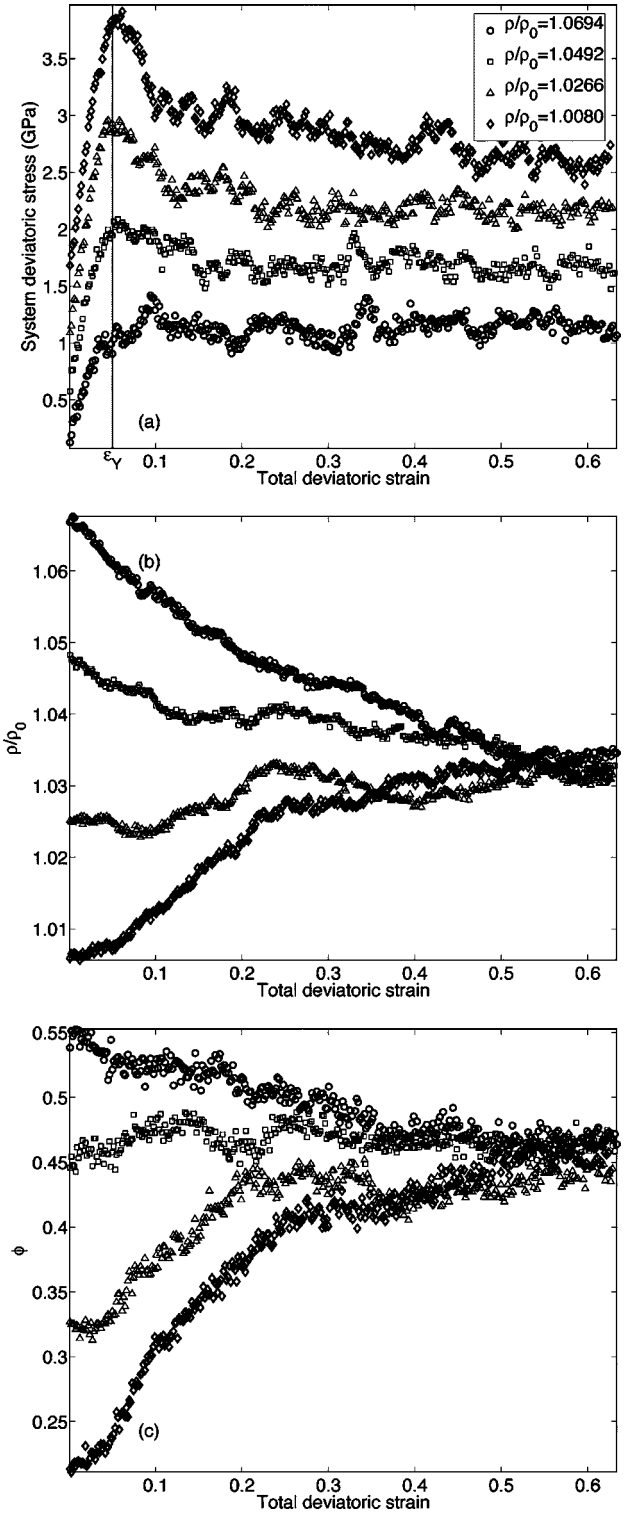

FIG. 15. The plots above show the variation of (a) deviatoric stress $\bar{\sigma}(\boldsymbol{\tau})$, (b) relative density ρ/ρ_0, and (c) mass fraction of liquidlike atomic environments ϕ as functions of the deviatoric component $\bar{\varepsilon}(\boldsymbol{\varepsilon})$ of the total externally applied strain for four a-Si structures of differing densities undergoing large-strain plastic flow under zero pressure. The data series in (a) all begin at the origin, but have been offset in increments of 0.5 GPa for clarity. Note that unlike in the case of deformation under constant volume (Fig. 10), all systems converge to a single value of ϕ characteristic of steady-state flow.

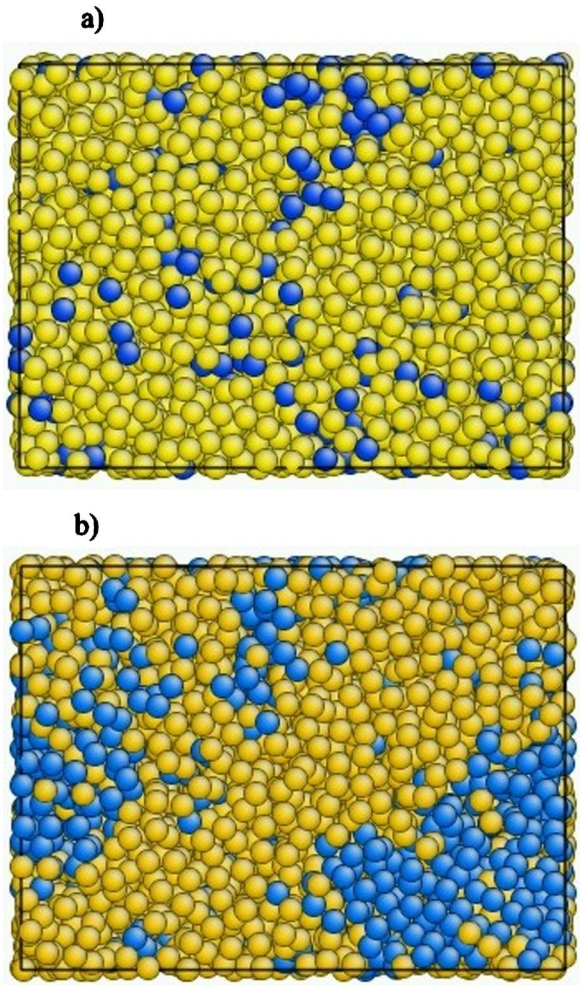

FIG. 16. (Color online) Visualization of a-Si systems with initially (a) high and (b) low liquidlike mass fractions of $\phi=0.55$ and $\phi=0.22$, respectively, after deformation to a total externally applied deviatoric strain of $\bar{\varepsilon}(\boldsymbol{\varepsilon})=0.12$. The environments of light-colored atoms have undergone transitions between solidlike and liquidlike form (or vice versa) during plastic flow, whereas those of the dark-colored atoms have not. Structure transitions in the a-Si system of low initial ϕ appear to localize into a relatively well-defined zone (b), but are distributed homogeneously in the a-Si system of high initial ϕ (a).

ties and that the overall properties of a bulk a-Si sample can be accurately determined from its overall mass fraction of liquidlike atomic environments ϕ by the rule of mixtures. It should therefore be possible to confirm the existence of these two environments by measuring the dependence of the properties of a-Si as a function of the quench rate at which it was created. Because of the fast crystallization kinetics of Si, however, bulk a-Si is typically made by techniques other than quenching,[27] e.g., by ion implantation.[44] Comparison of the results presented here to the properties of a-Si samples created by those methods is not straightforward because the degree of relaxation of those samples is difficult to correlate to that of a-Si created by fast quenching in the computer.

One possible method of circumventing this obstacle is to gauge the evolution of the properties of thoroughly annealed

a-Si (corresponding to the slowest-quenched a-Si samples presented in this study) during large-strain plastic flow. Unfortunately, there are few experiments that directly address this phenomenon. Witvrouw and Spaepen[75] conducted detailed analyses of the mechanisms of viscoelastic relaxation in a-Si, but only for strains on the order of a few percent, i.e., within the predicted elastic range a-Si [Fig. 10(a)] and too small to cause shear-induced transformations to the liquidlike form of a-Si. Part of the reason for the relatively low strains attained in these experiments is that bulk a-Si—like most ceramics—is intrinsically brittle: application of higher strains would likely have caused fracture in the samples under investigation. This limitation can, in principle, be circumvented if enough care is taken to reduce the number of possible crack nucleation sites and prevent the development of high tensile stresses under loading.

One approach that fulfills both criteria is to carry out an indentation study. Clarke *et al.* pursued this avenue[76] by using indentation of initially perfect c-Si to create fully dense a-Si. They then once again indented the amorphized region, causing a measurable increment of plastic flow under the indenter. In the course of indentation, the conductivity of a-Si under the indenter was observed to increase, indicating that the easily flowing state is metallic. Since liquid Si is metallic and denser than its diamond cubic crystalline form at the melting temperature,[56] this finding is consistent with the atomic structure of a-Si under indentation being "liquidlike." Upon unloading, however, the conductivity returned to its initial value and the structure of a-Si in the indented region could not be distinguished from its character before indentation. These findings imply that the easily flowing liquidlike state anneals out very quickly at the temperatures considered by Clarke *et al.*[76] or becomes unstable at low-enough pressures. The further study of flow in a-Si by indentation would therefore seem to require the development of *in situ* characterization techniques.

The discussion presented above concerned investigations of shear flow in a-Si. The possible existence of distinct solidlike and liquidlike amorphous forms in a-Si can also be studied by compressive loading. Such investigations were carried out on the behavior of a-Si and a-Ge for pressurization in anvil cells by Shimomura *et al.*[77] They found that both a-Si and a-Ge undergo sharp transitions to a more highly conducting state when condensed to pressures of 10 and 6 GPa, respectively. Using the same reasoning as was applied before in the case of flow under indentation, this observation is consistent with the high-pressure state being liquidlike. Unloading, however, was accompanied by a return to a state of lower conductivity and density for both a-Si and a-Ge and by crystallization in the case of a-Ge. Thus, these compression studies once again bring up the issue of the rate of "annealing-out" of the high-pressure metallic material or its possible instability at atmospheric pressure. Moreover, they suggest the possibility that the compressed conducting state is actually one of the well-known high-pressure crystalline metallic polymorphs of Si or Ge (Ref. 78) and, therefore, not amorphous (and by consequence not liquidlike).

The question of the rate of annealing-out of the dense conducting state of a-Si and a-Ge is difficult to investigate by atomistic simulations, since those are typically capable of accessing time scales on the order of only nanoseconds. Times on the order of micro- or milliseconds are completely beyond current capabilities for simulating amorphous solids, but are, nonetheless, short by experimental standards. One possible avenue for a future study of the kinetics of structural relaxation by atomistic simulation would be to extract a phenomenological spectrum of activation energies by using the scaling argument applied by Deng *et al.*[19] The degree of annealing-out of liquidlike material at room temperatures could then be estimated under the relatively conservative assumption that the mechanisms of relaxation and the ordering of their activation are the same regardless of the simulation time and temperature. The second question, concerning the possibility of the high-pressure state being crystalline, was addressed in experiments on a-Si by Deb *et al.*[79] who characterized the compressed conducting state found by Shimomura *et al.*[77] using *in situ* Raman spectroscopy. They determined that high-pressure a-Si is indeed amorphous and not crystalline, but were not able to provide more detailed information that could be compared against the quantities in Table II.

Because of a lack of experimental results, therefore, the quantities characterizing the two atomic environments of a-Si (Table II) cannot currently be confirmed directly. The trends they show, however, can be compared to those present in other amorphous solids that exhibit solidlike and liquidlike structures and whose properties have been closely studied. An example is provided by AlGe alloy, which forms two distinct amorphous structures upon compression in an anvil cell, including a dense conducting one.[80] Unlike in a-Si, however, both amorphous forms of a-AlGe remain metastable at room temperature and pressure, allowing them to be characterized in detail. Investigation by TEM and electron diffraction showed that these two forms are well described as solidlike and liquidlike, respectively.

Yvon *et al.*[80] chose to study AlGe alloy as a material that may exhibit solidlike and liquidlike amorphous structures on the basis that one of the components (Ge) has an open crystalline structure and contracts upon melting. This reasoning was based on the conjecture that these properties underlie the similarities in behavior of many directionally bonded materials, such as Si, Ge, H_2O, and SiO_2,[57] including the possible existence of multiple distinct amorphous forms. In particular, experimental findings have confirmed the existence of two distinct forms of amorphous H_2O that differ markedly in density.[81] The search for an underlying thermodynamic cause for the similarities among these substances has focused on the prospect of their exhibiting a liquid-liquid phase transition for sufficient undercooling below their melting temperatures.[40,82]

Comparing the liquidlike atomic environments found in SW a-Si defines an intriguing contrast with the characteristics of easily flowing material in metallic glasses, whose plastic flow behavior has been studied extensively. Regions of easy flow in metallic glasses are identified as those having a large "free volume" fraction.[19] They are sites where atomic motion is less constrained by close packing. The more easily flowing liquidlike a-Si, on the other hand, is denser than solidlike a-Si (Table II). It should be kept in mind, however,

that liquid silicon is denser than diamond cubic c-Si, whereas liquid metals are typically less dense than crystalline metals. Therefore, both liquidlike a-Si and regions of free volume in metallic glasses share the characteristic of being more similar in their local structures to the molten form of their constituent material than solidlike a-Si and the less easily flowing regions of metallic glasses, respectively. This commonality suggests that the liquidlike-solidlike distinction might be a more robust method of identifying easily flowing regions than free volume alone and may prove useful in the study of plasticity in amorphous materials other than a-Si.

Inroads into the study of local solidlike ordering in model two-dimensional metallic glasses have recently been made by Shi and Falk.[83] Their findings confirm the same trends in the quench rate dependence of yielding behavior as were discussed in the original exposition of the research presented here.[26] Furthermore, regions of short-range quasi-crystal-like order seem to play a similar role in their findings to the one played by solidlike atomic environments in a-Si, both with respect to overall mechanical behavior as well as flow localization. It is not clear, however, whether the quasi-crystal-like regions found by Shi and Falk are unambiguously discernable from other types of atomic environments, as are solidlike and liquidlike regions in a-Si (Sec. V). Neither physical properties, such as densities or average coordinations, nor structural characterizations by radial or bond-angle distribution functions of such quasi-crystal-like regions are known. Finally, the question of whether the mechanical behavior of three-dimensional metallic glasses can be described in terms of regions of local quasi-crystal-like structure has not yet been addressed.

In Sec. IX it was hypothesized that the mechanism of plastic deformation in a-Si is a localized structure transformation that initiates when a local yielding criterion is met. Similar behavior has been postulated for metallic glasses[19] and amorphous polymers.[25] Furthermore, Fig. 10 reveals that the steady-state flow levels of deviatoric stress in a-Si under constant volume deformation differ noticeably for the four initial structures of differing density. This effect is not observed under constant pressure deformation (Fig. 15), suggesting a direct dependence of the critical stress for initiation of localized shear transformations on pressure and ϕ.[84] A full investigation of the mechanisms of plasticity in a-Si that addresses the above hypotheses has been conducted by the authors and presented in a companion communication.[50]

Finally, in the Introduction to this paper, it was noted that this study of plasticity in a-Si was motivated by the unexpectedly high resistance to plastic flow of intergranular material in covalently bonded ceramic composite coatings, such as nc-TiN/a-Si_3N_4. The insight gained into the form of easily flowing material in a-Si can now be used in conjunction with studies conducted previously on the structure of intergranular material in SW nanocrystalline Si (nc-Si) to propose a reason for this high plastic flow resistance. Keblinski *et al.* showed that for certain high-energy grain boundary configurations,[38] the intergranular material in nc-Si is amorphous.[39] It is therefore characterizable by a liquidlike mass fraction ϕ. For intergranular material in nc-Si, however, the RDFs provided by Keblinski *et al.* are very closely comparable to those of the solidlike c-Si identified in this study (Fig. 7), indicating a very low value of ϕ. This material would therefore be highly resistant to plastic flow as a result of the local structure of its atomic environments.

XI. CONCLUSIONS

It has been demonstrated by molecular-dynamics simulation that SW a-Si contains two distinct forms of atomic environments. Because of the similarity of their configurations to the structure of silicon in its diamond cubic and molten states, these two environments are referred to as solidlike and liquidlike, respectively. The physical properties of any given a-Si sample can be characterized by the mass fraction ϕ of liquidlike atomic environments in it. In particular, ϕ acts as a plasticity carrier in a-Si. When plastically deformed at low temperatures, samples depleted of liquidlike environments exhibit a pronounced yield phenomenon followed by strain softening due to creation of new liquidlike environments by inelastic structure transformations. Samples with an initially high ϕ do not show any yield phenomenon before steady-state plastic flow is attained. When plastically deformed at low temperature under constant externally applied pressure, a-Si samples of differing initial ϕ converge to a single state of steady flow characterized uniquely by a specific average volume and ϕ.

ACKNOWLEDGMENTS

We would like to thank the Interfacial Materials Group at Argonne National Laboratory, specifically D. Wolf, P. Keblinski, and V. Yamakov, for making their MD codes available to us and for much helpful insight. We are also indebted to S. Veprek, N. Marzari, M. Bazant, S. Yip, J. Li, G. Ceder, H. E. Stanley, R. Sharma, and M. Zimmermann, for many useful discussions. This paper is based on work supported by the NSF Graduate program and by the Defense University Research Initiative on NanoTechnology (DURINT) on "Damage- and Failure-Resistant Nanostructured and Interfacial Materials," funded at the Massachusetts Institute of Technology by the Office of Naval Research under Grant No. N00014-01-1-0808.

*Corresponding author. Email address: demkowicz@lanl.gov

[1] S. Veprek, J. Vac. Sci. Technol. **17**, 2401 (1999).

[2] A. S. Argon and S. Veprek, Mater. Res. Soc. Symp. Proc. **697**, P1.2 (2002).

[3] A. Niederhofer, T. Bolom, P. Nesladek, K. Moto, C. Eggs, D. S. Patil, and S. Veprek, Surf. Coat. Technol. **146**, 183 (2001).

[4] Q. Ren, B. Joos, and M. S. Duesbery, Phys. Rev. B **52**, 13223 (1995).

[5] E. O. Hall, Proc. Phys. Soc. London, Sect. B **64**, 747 (1951).
[6] N. J. Petch, J. Iron Steel Inst., London **174**, 25 (1953).
[7] V. Yamakov, D. Wolf, S. R. Phillpot, A. K. Mukherjee, and H. Gleiter, Acta Mater. **49**, 2713 (2001).
[8] V. Yamakov, D. Wolf, S. R. Phillpot, A. K. Mukherjee, and H. Gleiter, Nat. Mater. **1**, 1 (2002).
[9] J. Schiotz and K. W. Jacobsen, Science **301**, 1357 (2003).
[10] J. Schiotz, Scr. Mater. **51**, 837 (2004).
[11] S. Yip, Nature (London) **391**, 532 (1998).
[12] J. Schiotz, F. D. Di Tolla, and K. W. Jacobsen, Nature (London) **391**, 561 (1998).
[13] S. Veprek and S. Reiprich, Thin Solid Films **268**, 64 (1995).
[14] A. C. Lund and C. A. Schuh, Mater. Res. Soc. Symp. Proc. Vol. **806**, MM7.4.1 (2004).
[15] A. S. Argon and H. Y. Kuo, Mater. Sci. Eng. **39**, 101 (1979).
[16] K. Maeda and S. Takeuchi, Philos. Mag. A **44**, 643 (1981).
[17] D. Srolovitz, V. Vitek, and T. Egami, Acta Metall. **31**, 335 (1983).
[18] A. S. Argon and L. T. Shi, in *Amorphous Materials: Modeling of Structure and Properties*, edited by V. Vitek, Metallurgical Society of AIME, Warrendale, PA, p. 279, 1983.
[19] D. Deng, A. S. Argon, and S. Yip, Philos. Trans. R. Soc. London, Ser. A **329**, 549 (1989); **329**, 575 (1989); **329**, 595 (1989); **329**, 613 (1989).
[20] V. V. Bulatov and A. S. Argon, Modell. Simul. Mater. Sci. Eng. **2**, 167 (1994); **2**, 185 (1994); **2**, 203 (1994).
[21] M. L. Falk and J. S. Langer, Phys. Rev. E **57**, 7192 (1998).
[22] D. N. Theodorou and U. W. Suter, Macromolecules **18**, 1467 (1985).
[23] D. N. Theodorou and U. W. Suter, Macromolecules **19**, 379 (1986).
[24] M. Hutnik, A. S. Argon, and U. W. Suter, Macromolecules **26**, 1097 (1993).
[25] P. H. Mott, A. S. Argon, and U. W. Suter, Philos. Mag. A **67**, 931 (1993).
[26] M. J. Demkowicz and A. S. Argon, Phys. Rev. Lett. **93**, 025505 (2004).
[27] K. Tanaka, *Amorphous Silicon* (Wiley, New York, 1999).
[28] K. Furukawa, M. Shimbo, K. Fukuda, and K. Tanzawa, *Extended Abstracts of the 18th (1986 International) Conference on Solid-State Devices and Materials*, Tokyo, B-9-1, pp. 533–536, 1986.
[29] S. Veprek, Z. Iqbal, H. R. Oswald, and A. P. Webb, J. Phys. C **14**, 295 (1981).
[30] T. D. Shen, C. C. Koch, T. L. McCormick, R. J. Nemanich, J. Y. Huang, and J. G. Huang, J. Mater. Res. **10**, 139 (1995).
[31] S. Hao, B. Delley, and C. Stampfl (unpublished).
[32] F. H. Stillinger and T. A. Weber, Phys. Rev. B **31**, 5262 (1985).
[33] J. Tersoff, Phys. Rev. Lett. **56**, 632 (1986).
[34] H. Balamane, T. Halicioglu, and W. A. Tiller, Phys. Rev. B **46**, 2250 (1992).
[35] M. Z. Bazant, E. Kaxiras, and J. F. Justo, Phys. Rev. B **56**, 8542 (1997).
[36] W. D. Luedtke and U. Landman, Phys. Rev. B **40**, 1164 (1989).
[37] M. D. Kluge and J. R. Ray, Phys. Rev. B **37**, 4132 (1988).
[38] P. Keblinski, S. R. Phillpot, D. Wolf, and H. Gleiter, Phys. Rev. Lett. **77**, 2965 (1996).
[39] P. Keblinski, S. R. Phillpot, D. Wolf, and H. Gleiter, Acta Mater. **45**, 987 (1997).
[40] S. Sastry and C. A. Angell, Nat. Mater. **2**, 739 (2003).
[41] P. N. Keating, Phys. Rev. **145**, 637 (1966).
[42] Y. Waseda and K. Suzuki, Z. Phys. B **20**, 339 (1975).
[43] P. Keblinski, M. Z. Bazant, R. K. Dash, and M. M. Treacy, Phys. Rev. B **66**, 064104 (2002).
[44] K. Laaziri, S. Kycia, S. Roorda, M. Chicoine, J. L. Robertson, J. Wang, and S. C. Moss, Phys. Rev. Lett. **82**, 3460 (1999).
[45] W. Cai, V. V. Bulatov, J. F. Justo, A. S. Argon, and S. Yip, Phys. Rev. Lett. **84**, 3346 (2000).
[46] M. P. Allen and D. J. Tildesley, *Computer Simulation of Liquids* (Oxford University Press, Oxford, London, 2000).
[47] M. Parinello and A. Rahman, Phys. Rev. Lett. **45**, 1196 (1980).
[48] H. C. Andersen, J. Chem. Phys. **72**, 2384 (1980).
[49] M. Hutnik, A. S. Argon, and U. W. Suter, Macromolecules **24**, 5970 (1991).
[50] M. J. Demkowicz and A. S. Argon, following paper, Phys. Rev. B **72**, 245206 (2005).
[51] F. A. McClintock and A. S. Argon, *Mechanical Behavior of Materials* (Addison-Wesley, Reading, MA, 1966).
[52] D. Brown and S. Neyertz, Mol. Phys. **84**, 577 (1995).
[53] K. Maeda and S. Takeuchi, J. Phys. F: Met. Phys. **12**, 2767 (1982).
[54] S. R. Phillpot, S. Yip, and D. Wolf, Comput. Phys. **2**, 20 (1989).
[55] J. Q. Broughton and X. P. Li, Phys. Rev. B **35**, 9120 (1987).
[56] V. M. Glazov, S. N. Chizhevskaya, and N. N. Glagoleva, *Liquid Semiconductors* (Plenum, New York, 1969) Ch. 3.
[57] C. A. Angell, S. Borick, and M. Grabow, J. Non-Cryst. Solids **205–207**, 463 (1996).
[58] G. T. Barkema and N. Mousseau, Phys. Rev. Lett. **77**, 4358 (1996).
[59] X. Jiang, B. Goranchev, K. Schmidt, P. Grunberg, and K. Reichelt, J. Appl. Phys. **67**, 6772 (1990).
[60] D. Turnbull and M. H. Cohen, J. Chem. Phys. **34**, 120 (1961).
[61] M. H. Cohen and G. S. Grest, Phys. Rev. B **20**, 1077 (1979).
[62] S. Torquato, *Random Heterogeneous Materials* (Springer-Verlag, New York, 2002).
[63] B. Lu and S. Torquato, J. Chem. Phys. **93**, 3452 (1990).
[64] G. Rasigni, F. Varnier, M. Rasigni, J. P. Palmari, and A. Llebaria, Phys. Rev. B **27**, 819 (1983).
[65] D. N. Theodorou and U. W. Suter, Macromolecules **18**, 1206 (1985).
[66] R. Zallen, in *Fluctuation Phenomena*, edited by E. W. Montroll (North-Holland, Amsterdam, 1979).
[67] W. H. Zachariasen, J. Am. Chem. Soc. **54**, 3841 (1932).
[68] G. S. Cargill, in *Solid State Physics V.30*, edited by H. Ehrenreich, F. Seitz, and D. Turnbull (Academic Press, New York, 1975).
[69] J. D. Bernal, Proc. R. Soc. London, Ser. A **280**, 299 (1964).
[70] A. S. Argon, "Mechanical Properties of Single-Phase Crystalline Media: Deformation at Low Temperatures," in *Physcial Metallurgy*, edited by R. W. Cahn and P. Haasen (North-Holland, Amsterdam, 1996), Ch. 21.
[71] D. J. Safarik, C. M. Cady, and R. B. Schwarz, Acta Mater. **53**, 2193 (2005).
[72] H. Alexander and P. Haasen, in *Solid State Physics*, edited by F. Seitz (Academic Press, New Yor, 1968), Vol. 22.
[73] L. Anand and M. E. Gurtin, Int. J. Solids Struct. **40**, 1465 (2003).
[74] L. Anand and C. Su, J. Mech. Phys. Solids **53**, 1362 (2005).
[75] A. Witvrouw and F. Spaepen, J. Appl. Phys. **74**, 7154 (1993).
[76] D. R. Clarke, M. C. Kroll, P. D. Kirchner, and R. F. Cook, Phys. Rev. Lett. **60**, 2156 (1988).
[77] O. Shimomura, S. Minomura, N. Sakai, and K. Asaumi, Philos. Mag. **29**, 547 (1974).

[78] D. A. Young, *Phase Diagrams of the Elements* (University of California Press, Berkeley, 1991).
[79] S. K. Deb, M. Wilding, M. Somayazulu, and P. F. McMillan, Nature (London) **414**, 528 (2001).
[80] P. J. Yvon, R. B. Schwarz, D. Schiferl, and W. L. Johnson, Philos. Mag. Lett. **72**, 167 (1995).
[81] O. Mishima, L. D. Calvert, and E. Whalley, Nature (London) **314**, 76 (1985).
[82] H. E. Stanley, C. A. Angell, U. Essmann, M. Hemmati, P. H. Poole, and F. Sciortino, Physica A **205**, 122 (1994).
[83] Y. Shi and M. L. Falk, Phys. Rev. Lett. **95**, 095502 (2005).
[84] A. S. Argon and L. T. Shi, Acta Metall. **31**, 499 (1983).